Strain transfer in ferroelectric-ferrimagnetic magnetoelectric composite

Sujoy Saha, Ram Prakash Singh, Ying Liu, Atal Bihari Swain, Amritesh Kumar, V. Subramanian, A. Arockiarajan, G. Srinivasan, and Rajeev Ranjan

Phys. Rev. B **103**, L140106 — Published 22 April 2021

DOI: 10.1103/PhysRevB.103.L140106

Strain transfer in ferroelectric-ferrimagnetic magnetoelectric composite

Sujoy Saha[1], Ram Prakash Singh[1], Ying Liu[2,3], Atal Bihari Swain[4], Amritesh Kumar[5], V. Subramanian[4], A. Arockiarajan[5], G. Srinivasan,[2] and Rajeev Ranjan[1]*

[1]Department of Materials Engineering, Indian Institute of Science, Bangalore-560012, India

[2]Department of Physics, Oakland University, Rochester, MI 48309-4479, USA

[3]Department of Materials Science and Engineering, Hubei University, Wuhan 430062, China

[4]Department of Physics, Indian Institute of Technology Madras, Chennai-600036, India

[5]Department of Applied Mechanics, Indian Institute of Technology Madras, Chennai-600036, India

Abstract

We show that electrically poled ferroelectric matrix considerably enhances the localized magnetostrictive deformations in a ferroelectric-ferrimagnetic composite. Magneto-strain measurements performed on Dy-free and Dy-modified $BiFeO_3$-$PbTiO_3$ (BF-PT) ferroelectric ceramics revealed no measurable macroscopic strain in poled and unpoled Dy-free non-ferromagnetic specimens. Dy-modified BF-PT, on the other hand, exhibit ferrimagnetic dysprosium iron garnet (DyIG) as precipitates and exhibit a macroscopic strain of - 4 ppm in the poled state. Despite the small (6 %) volume fraction of DyIG, the macroscopic strain in Dy-modified BF-PT is almost 50 % of the strain of pure DyIG. Our results suggest that the amplification of the localized magnetostrictive deformation in the FM islands by the neighboring ferroelectric regions is caused by the magnetostrictive stress induced motion of ferroelectric-ferroelastic domains of the poled ferroelectric matrix.

* rajeev@iisc.ac.in

The discovery of the ability to pole a dense polycrystalline ferroelectric ceramic by electric field and make it behave like a piezoelectric material is considered as one of the important milestones in the history of piezoelectricity [1]. While, on the one hand, it made possible robust and low cost piezoceramics available as actuators, pressure sensors and transducers in wide ranging applications spanning sectors like medical diagnostics, space, telecommunication, defense, automobiles, etc. [2], it also stimulated scientific curiosity as to how ferroelectric domain walls (generally considered to be crystallographic planes) move across large scale interruptions (such as the grain boundaries) in dense polycrystalline piezoelectric materials [3-5]. As compared to their single crystal counterparts, polycrystalline solids exhibit special features like residual stress/strain on mesoscopic length scales due to the combined effect of anisotropic thermal expansion and clamping of the randomly oriented grains. Additional contribution to strain heterogeneity comes into picture in ferroelectric ceramics due to onset of the spontaneous lattice strain as the body cools through the Curie point after densification at high temperatures [6-8]. The inhomogeneous strain introduces complex domain configuration [9] which, perhaps, aid in increasing the probability of finding compatible domains across the grain boundaries for easy switching, not feasible otherwise [10].

In most experiments, the global response (polarization/strain) of an electrically poled ferroelectric body is measured after excitation with a macroscopic external stimulus (electric field/stress). An interesting question to ask is *how local stimuli within the interior of the system would make the ferroelectric system respond on the global scale?* Such a study would offer insight into the role of domain alignment in the transference of the signal from the embedded local source to the surrounding ferroelectric phase, and its eventual manifestation on the global scale. Ferroelectric (FE)-ferro/ferrimagnetic (FM) magnetoelectric particulate composites can serve as model systems to investigate this question. In recent past such composites have received considerable attention for their ability to exhibit large magnetoelectric (ME) coupling as compared to their single-phase counterparts [11-16]. The magnetoelectric coupling in a ferroelectric-ferrimagnetic composite is strain mediated wherein the magnetostrictive (piezoelectric) strain is transferred from the ferromagnetic (piezoelectric) phase to the piezoelectric (ferromagnetic) phase affecting the state of polarization (magnetization). Although to achieve large ME coupling 1:1 volume fraction of the FM and FE phases is desired [11], for the purpose of our study, we prefer very small volume fraction of the FM phase to minimize the contribution of the cumulative deformations in the FM grains to the measured macroscopic strain of the composite. The strategy for making such a specimen was borrowed

from our earlier work [17, 18] wherein it was possible to precipitate small volume fraction of ferrimagnetic phase in a uniform manner across the sample volume by use of additives.

The nominal composition of the ferroelectric specimen was $0.66Bi_{0.90}Dy_{0.10}FeO_3$-$0.34PbTiO_3$ (designated as 34PTDy10). The details of the specimen preparation can be found in the Supplemental Material [19]. Back-scattered scanning electron microscopy image (Fig. 1(a)) reveals two distinctly different types of grains. Though on occasions, small grains (~2 μm) can be seen within the large grains (~ 12 μm), they are mostly located between boundaries of the large grains. Image analysis using the standard ASTM protocol [20] suggests the small grains to occupy ~6% of the specimen volume. A line scan energy dispersive x-ray (EDX) analysis revealed an abrupt increase in the atomic concentrations of Dy and Fe in the small grain, Fig. 1(b). The average atomic ratio of Dy:Fe (as determined from EDX analysis over large number of small grains) was found to 3.15 : 5.19 and is close to the atomic ratio expected for $Dy_3Fe_5O_{12}$, i.e. dysprosium-iron garnet (DyIG). Electron diffraction study of a region comprising a small grain adjacent to a big grain confirmed the small grain to be DyIG, Fig. 1(c). This was further confirmed by Rietveld analysis of the x-ray powder diffraction pattern (Fig. 1(d)) which revealed only the perovskite and garnet phases with volume fraction of DyIG phase ~6%, in conformity with the ASTM analysis. Cyclic polarization-electric field (*P*-*E*), magnetization-magnetic field (*M*-*H*) and electrostrain (*s*-*E*) measurements (Fig. 2) confirmed the 34PTDy10 specimen to exhibit both ferroelectric and ferromagnetic behavior. The magnetization at 2 kOe is ~ 0.2 emu/gm which is ~ 5 % of the value of polycrystalline DyIG (Fig. 4d). The poled specimen of 34PTDy10 shows longitudinal piezoelectric coupling coefficient 72 *pC/N* which was stable with time. The linear *M*-*H* response of the Dy free specimen, i.e., $0.66BiFeO_3$-$0.34PbTiO_3$ (34PTDy0), confirmed that the perovskite phase does not contribute to the ferromagnetic behavior (Fig. S1, Supplemental Material [19]). This conclusion was further reinforced when we found a nearly linear M-H response of the magnetically separated powders of 34PTDy10 (for details please refer to Fig. S2, Supplemental Material [19]).

To check if the specimen exhibits ME coupling, we performed magnetoelectric (ME) coupling measurements on the electric poled specimen both in the quasi-static and at the electromechanical resonance frequency using ac magnetic signal of 1 Oe (for the details of ME measurements please refer to Fig. S3 in Ref. [19]). The quasi-static measurement was performed as a function of a superposed DC field (H_{dc}), Fig. 3(a). The maximum α of ~5.6 mV/cm-Oe was obtained at a dc field of ~100 Oe, close to the coercive field. However, beyond

H_c, α decreases very slowly with increasing H_{dc}. This behaviour contrasts with most reports wherein α decrease significantly for H_{dc} above the H_c [21, 22]. The slow variation of α with H for our specimen is consistent with the very small volume fraction of the FM phase (DyIG) [11]. For α measurements at the electromechanical resonance, the resonance frequency was first determined using impedance measurement, Fig. 3(b). The specimen was subsequently excited with low amplitude H_{ac} field close to the electromechanical resonance frequency. The peak α was found to be ~2100 mV/cmOe^{-1} at ~240 kHz, Fig. 3(c). One of present authors have previously reported very large α~10^4 mv/cm-Oe in a composite specimen using nearly 60 volume fraction $Ni_{0.8}Zn_{0.2}Fe_2O_4$ as the FM phase and PZT as the ferroelectric phase [23]. The lower α of our specimen both in the quasi-static and resonance measurements is consistent with the low volume fraction of the FM phase and its relatively one order lower magnetostriction as compared to those of the spinel ferrites [24, 25].

Though from the property perspective the specimen shows comparatively low magnetoelectric coupling, the small volume fraction of the FM phase makes this system most suitable to investigate the nature of strain transfer from the FM phase to the FE phase. The precipitation of the FM phase in such a small volume fraction, and their lack of interconnectedness across the sample volume is unlikely to show a measurable magnetostriction on the global scale. To check this, we carried out strain measurements as a function of (bipolar) magnetic field on 34PTDy10 pellet using a resistance strain gauge fixed on top of a circular disc of about 12 mm diameter. Consistent with our anticipation, the unpoled specimen shows no measurable strain (*s*) with magnetic field (*H*), Fig. 4(a). Interestingly, however, the poled specimen exhibits strain of ~4 ppm at 2 kOe. We may note that the *s*-*H* were performed after aging the poled specimen for 25 days to exclude the possibility of the contribution of polarization/domain relaxation in the measured strain. For reference sake, we performed *s*-*H* measurements on a poled Dy-free specimen (34PTDy0) and found no measurable strain (Fig. 4(a)).

A comparison of the *s*-*H* plots of 34PTDy10 and pure polycrystalline DyIG (synthesized separately for reference measurement, Fig. 4(b)) offers fundamental insights regarding the mechanism associated with the strain developed in poled 34PYDy10 with magnetic field. (i) Even though the DyIG phase in 34PTDy10 merely 6 volume percent, the magnitude of its strain (say ~4 ppm at 2 kOe) is nearly half the strain (~8 ppm) exhibited by pure polycrystalline DyIG. (ii) While the strain is reversible for DyIG during the increasing and decreasing *H*, 34PTDy10 shows a large remanence strain s_R when *H* is reduced to zero.

(iii) In the negative half of the *s-H* measurement, strain in 34PTDy10 increases again from its remanent value and returns to the remanence following a weak hysteresis, Fig. 4(c). In contrast, within the resolution of our measurement, no hysteretic behavior was observed for the DyIG specimen. The non-hysteretic *s-H* behavior of DyIG suggests the measured strain of this specimen is a lattice phenomenon. This is not the case with poled 34PTDy10. Since the magnetostrictive contribution of the 6 % of the DyIG phase in 34PTDy10 is insignificant, the measured macroscopic strain is solely due to cumulative deformation of the poled ferroelectric grains caused by localized stress fields generated by randomly distributed small islands of the DyIG phase. The remanence and the hysteretic behaviour of the *s-H* curve confirms that amplification process is associated with a cumulative motion of the ferroelectric-ferroelastic domain walls across the grain boundaries of ferroelectric grains, caused by cumulative action of the stress fields induced by the isolated FM islands.

The strain-magnetic field plot shown in Fig. 4a is analogous to the electrostrain behaviour of a normal ferroelectric specimen under unipolar electric-field cycling (starting from an unpoled specimen). The first exposure of electric field causes considerably large reorientation of the ferroelectric-ferroelastic domains and large strain vis-à-vis the unpoled state. Since for normal ferroelectrics only a small fraction of the ferroelectric-ferroelastic domains back switch after the field is reduced to zero, the strain decreases slightly to a remanent value when electric field is reduced to zero. The strain in the subsequent unipolar cycles is relatively small and almost reversible in nature, determined solely by the fraction of the ferroelastic domains which can back switch. Our strain-magnetic field data shown in Fig. 4a mimics this scenario. On the first experience of cumulative stress from within (caused by local magnetostrictive deformation of the DyIG islands), the domains in the poled ferroelectric grains rearrange to give a large negative strain. The slight decrease in strain on reducing to magnetic-field to zero is due to back switching of small fraction of the ferroelectric-ferroelastic domains when the cumulative localized magnetostriction driven stress is reduced to zero. Since the magnetostrictive strain remains negative even when the sign of the magnetic field is reversed, the nature of the cumulative localized stress acting on the ferroelectric grains do not change on reversing the direction of magnetic field. Interesting to note that the effective linear magneto-strain coefficient $d\lambda/dH$ in the irreversible region of Fig. 4a is ~ 4 ppm/kOe. This value is close to the value obtained for DyIG (~ 4.5 ppm/kOe). For the reversible part, the coefficient is considerably reduced to ~0.2 ppm /kOe. The significant reduction in the reversible cycle is because the contribution to the strain (over the remanent value) is solely due

to the small fraction of the ferroelectric domains which can back switch to their configuration corresponding to the remanent strain state.

The ferroelectric phase of our specimen exhibits rhombohedral perovskite structure as evident from the split of the pseudocuic $\{111\}_{pc}$ Bragg profile. For this phase, the spontaneous polarization is along the [111] direction of the rhombohedral structure. Strong electric field would switch the most favourably oriented domains (in the different grains) towards the electric-field direction causing preferred orientation. The fraction of the domain reorientation, as estimated from the intensity ratio of the (11-1) and (111) peaks [26] before and after poling the pellet (Fig. S4, Supplemental Material [19]), is $\eta = 0.34$. In ferroelectrics, switching of ferroelastic domains cause large dimensional changes. In the context of perovskite-based ferroelectrics, there is a strong coupling between switching of ferroelastic domains and lattice strain along the non-polar directions [27] (Fig. S4, Supplemental Material [19]). In view of the fact that this coupling persists and ferroelectric-ferroelastic domain switching happen even below the coercive field [27], the observation of weak hysteresis in the cyclic *s*-*H* of 34PTDy10 (Fig. 4(c)) can be attributed to the underlying motion of ferroelastic domain walls in the ferroelectric grains. We attempted to capture this by monitoring the change in the relative intensity of the (11-1) and (111) rhombohedral peaks of the poled specimen after soaking the poled specimen in a magnetic field of ~10 kOe for ~1 hour. However, we did not see any noticeable change within the experimental resolution. Since the strain developed in the ferroelectric specimen by magnetic field is nearly two orders of magnitude smaller than the strain achieved by electric field (the specimen exhibits a longitudinal electrostrain ~0.05% at 70 kV/cm whereas the magnitude of the strain induced by the magnetic-field is merely 0.0004 %), the corresponding change in the relative intensity of the (11-1) and (111) peaks is expected to be very small, beyond the ability of our detection.

In summary, we investigated the phenomenon of strain transfer from ferro/ferrimagnetic (FM) islands to the ferroelectric (FE) matrix in a model magnetoelectric composite system comprising of small volume fraction of the FM phase. We discovered that the insignificantly small localized magnetostrictive deformations in the FM islands get considerably amplified by the poled FE matrix. The hysteretic nature of macroscopic strain proves that this amplification is associated with the cumulative motion of the ferroelectric-ferroelastic domain walls in the ferroelectric matrix under the influence of localized stress fields generated by magnetostrictive deformations in the embedded FM islands due to the external magnetic field. While offering insight regarding to how strain in the ferrimagnetic

phase couples to the strain in the ferroelectric phase in such composite magnetoelectric materials, our model experiment can also be used for better understanding of domain dynamics in ferroelectric systems when perturbed from within.

Acknowledgments: S. S. acknowledges CSIR, India for the Senior Research Associateship. R. P. S. thanks the PRMF Scheme of the Govt. of India. R. R. acknowledges the Nano mission Program of the Department of Science and Technology (Grant No. SR/NM/NS-1010/2015 (G)), Council of Scientific and Industrial Research (Grant No. 03 (1347)/16/EMR-II), and Science and Engineering Research Board (SERB) of the Ministry of Science and Technology (Grant No. EMR/2016/001457), Govt. of India for financial support. The research at Oakland University was supported by grants from the National Science Foundation (DMR-1808892, ECCS-1923732) and the Air Force Office of Scientific Research (AFOSR) Award No. FA9550-20-1-0114.

References

[1] Gene H. Haertling, J. Am. Ceram. Soc., **82**, 797 (1999).

[2] M. Gagliardy, Am. Ceram. Soc. Bull. **99**, 7 (2020).

[3] M. E. Lines, and A. M. Glass, *Principles and Applications of Ferroelectrics and Related Materials* (Oxford University Press, New York, 2001).

[4] S. Mantri, J. Oddershede, Dr. Damjanovic, and J. E. Daniels, Acta Mater. **128**, 400 (2017).

[5] D. M. Marincel , H. Zhang , A.Kumar , S. Jesse , S. V. Kalinin , W. M. Rainforth , I. M. Reaney , C. A. Randall, and S. T.McKinstry, Adv. Funct. Mater. **24**, 1409 (2014).

[6] M. J. Hoffman, M. Hammer, A. Endriss, and D. C. Lupascu, Acta Mater. **49**, 1301 (2001).

[7] D. A. Hall, A. Steuwer, B. Cherdhirunkorn, T. Mori, and P. J.Withers, Acta Mater. **54**, 3075 (2006).

[8] J. L. Jones, M. Hoffman, J. E. Daniels, and A. J. Studer, Appl. Phys. Lett. **89**, 092901 (2006).

[9] H. Simons, A. B. Haugen, A. C. Jakobsen, S. Schmidt, F. Stöhr, M. Majkut, C. Detlefs, J. E. Daniels, D. Damjanovic, H. F. Poulsen, Nat. Mat. **17**, 814 (2018).

[10] J. Y. Li, R. C. Rogan, E. U. Stundag, K. Bhattacharya, Nat. Mat. **4**, 776 (2005).

[11] C. -W. Nan, M. I. Bichurin, S. Dong, D. Viehland, and G. Srinivasan, J. Appl. Phys. **103**, 031101 (2008).

[12] H. Palneedi, V. Annapureddy, S. Priya, and Jungho Ryu, Actuators **5**, 9 (2016).

[13] M. Bichurin, V. Petrov, A. Zakharov, D. Kovalenko, S. C. Yang, D. Maurya, V. Bedekar, and S. Priya, Materials, **4**, 651 (2011).

[14] C. A. F. Vaz, J. Hoffman, C. H. Ahn, and R. Ramesh, Adv. Mater., **22**, 2900 (2010).

[15] C. -W. Nan, Phys. Rev. B **50**, 6082 (1994).

[16] C. -W Nan, M. Li, and Jin H. Huang, Phys. Rev. B **63**, 144415 (2001).

[17] S. Saha, R. P. Singh, A. Kumar, A. De, P. P., B. Narayan , H. Basumatary, A. Senyshyn, and Rajeev Ranjan, Appl. Phys. Lett. **116**, 142902 (2020).

[18] A. Kumar, A. Kumar, S. Saha, H. Basumatary, and Rajeev Ranjan, Appl. Phys. Lett. **114**, 022902 (2019).

[19] See Supplemental Material for experimental methods and other details.

[20] ASTM International, E562-19 Standard Test Method for Determining Volume Fraction by Systematic Manual Point Count (ASTM International, West Conshohocken, PA, 2019).

[21] Q. H. Jiang, Z. J. Shen, J. P. Zhou, Z. Shia, C. -W. Nan, J. Euro. Ceram. Soc. **27**, 279 (2007).

[22] C. -S. Park, and S. Priya, J. Am. Ceram. Soc. **94**, 1087 (2011).

[23] G. Srinivasan, C. P. DeVreugd, C. S. Flattery, V. M. Laletsin, and N. Paddubnaya, Appl. Phys. Lett. **85**, 2550 (2004).

[24] R. A. Islam, H. Kim, S. Priya, and H. Stephanou, Appl. Phys. Lett. **89**, 152908 (2006).

[25] G. Sreenivasulu, V. Hari Babu, G. Markandeyulu, and B. S. Murty, Appl. Phys. Lett. **94**, 112902 (2009).

[26] A. Pramanick, D. Damjanovic, J. E. Daniels, J. C. Nino, and J. L. Jones, J. Am. Ceram. Soc. **94**, 293 (2011).

[27] D. K. Khatua, Lalitha K. V., C. M. Fancher, J. L. Jones, and R. Ranjan, J. Appl. Phys. **120**, 154104 (2016).

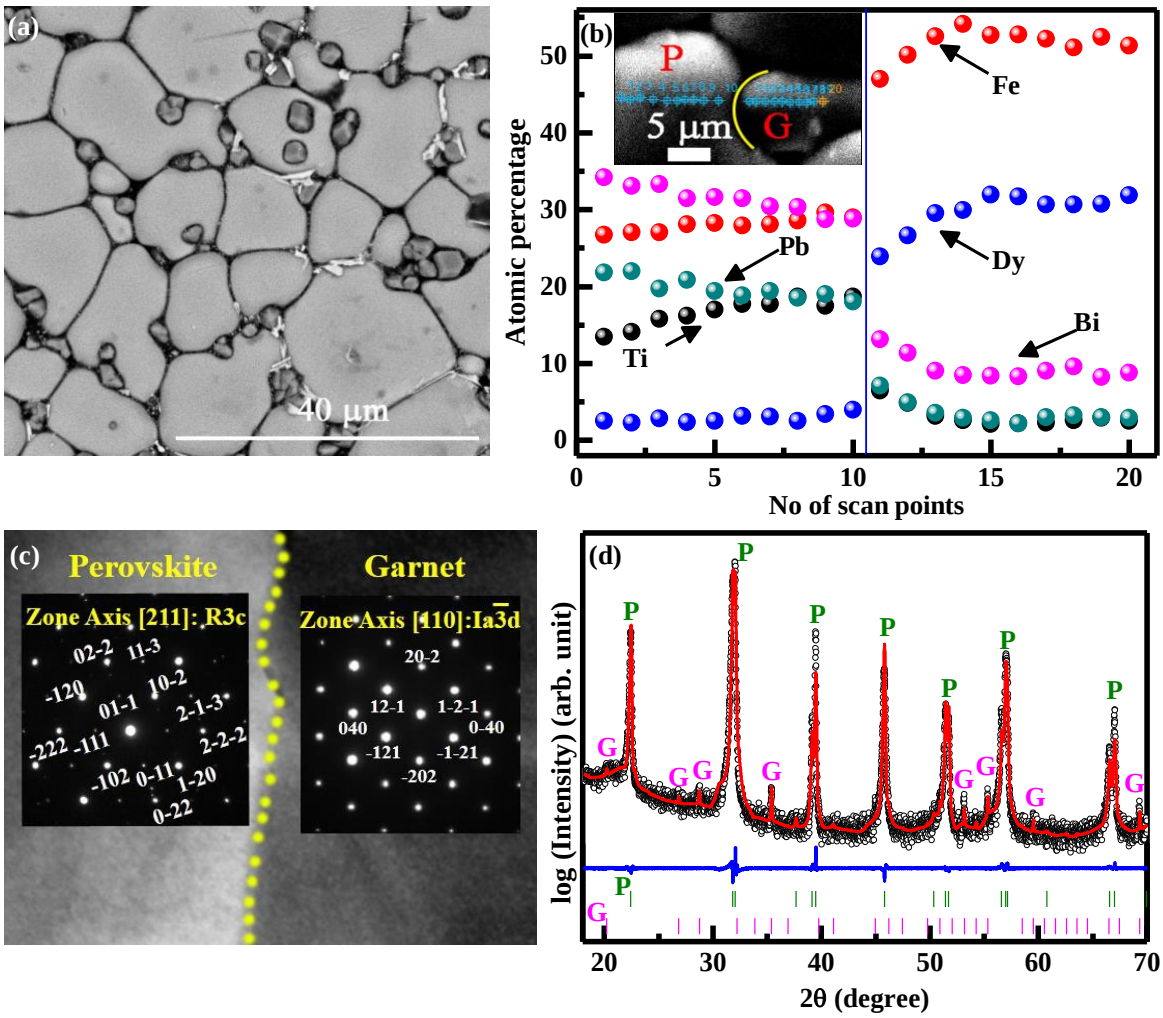

FIG. 1. (a) Back scattered SEM image of 34PTDy10. The perovskite grains have lighter contrast vis-á-vis darker garnet grains. (b) EDX line scan analysis across a boundary of large grain (P) and small grain (G). Note the abrupt increase in the atomic concentration of Dy and Fe in the G grain and a concomitant decrease in the intensity of Pb and Bi. (c) High-angle annular dark-field scanning transmission electron microscopy (HAADF-STEM) image of a large-small grain interface of 34PTDy10. The yellow dotted line indicates the interface between the two grains. The selected area electron diffraction (SAED) pattern is shown for the corresponding grains. The diffraction pattern on the left could be indexed by [211] zone axis of rhombohedral (R3c) perovskite structure. The electron diffraction pattern of the right grain on the other hand matched with the [110] zone axis of cubic garnet (DyIG) phase. (d) Rietveld fitted XRD pattern of 34PTDy10 with phase mixture of DyIG and rhombohedral (R3c) perovskite. The refined structural parameters are given in ref. [19] The open black circles represent the observed pattern and red solid line represents the fitted pattern. The blue solid line represents the difference between the observed and fitted pattern. Here the intensity is presented on a logarithmic scale to highlight the minor garnet peaks (designated as G, the Bragg positions are shown with magenta vertical lines). The perovskite peaks are designated as P, and the corresponding Bragg positions are denoted by green vertical lines. Apart from these two phases, there is no trace of any third phase.

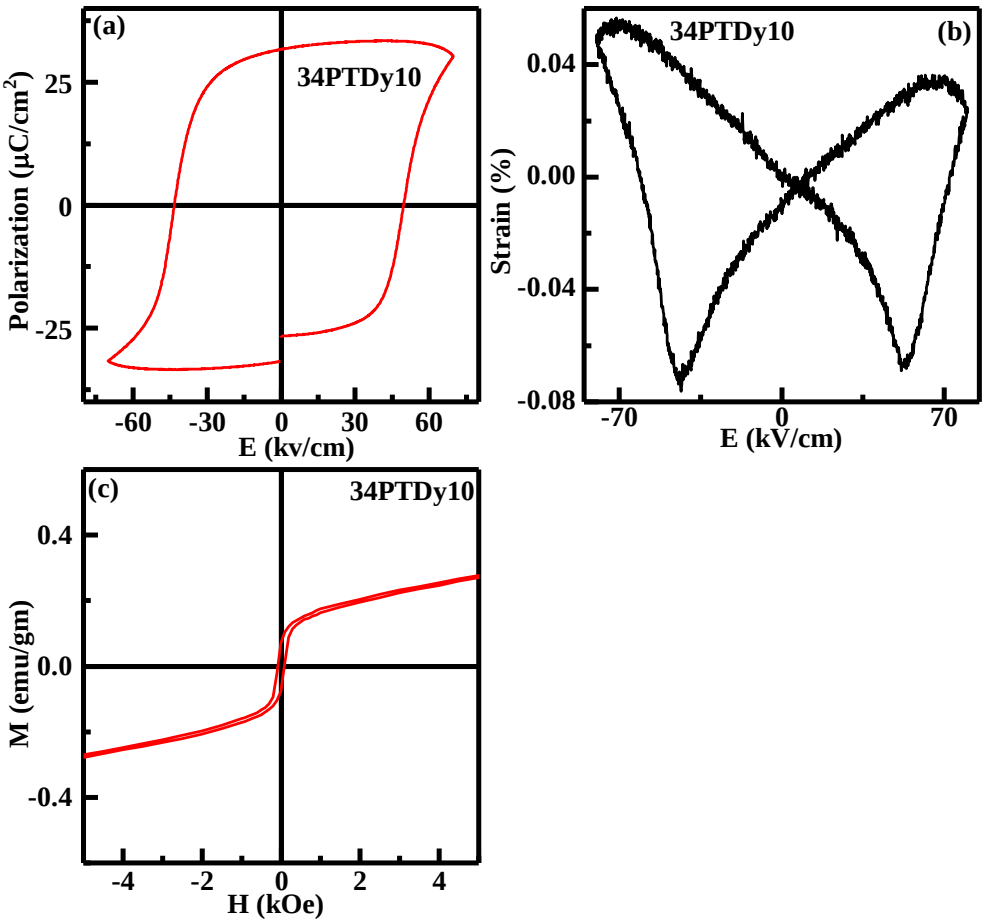

FIG. 2. (a) Polarization-electric field, (b) Strain-electric field and (c) magnetization-magnetic field curves of 34PTDy10.

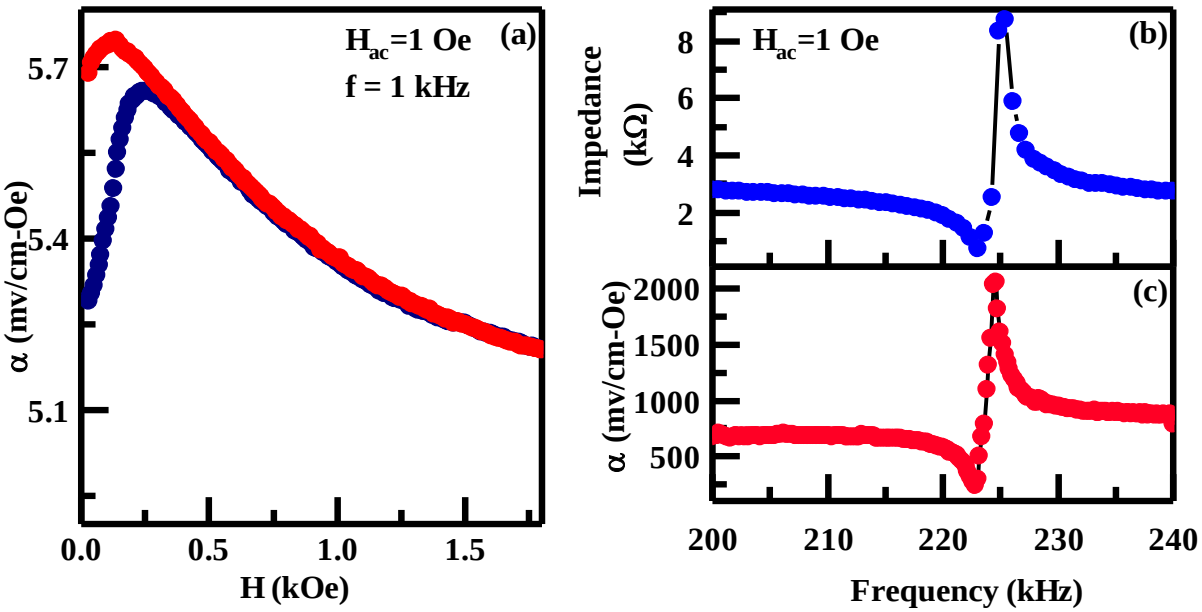

FIG. 3. (a) Variation of magnetoelectric coefficient (α) as a function of dc magnetic field of 34PTDy10. (b) Variation of impedance of poled 34Dy10 as a function of frequency. (c) Variation of magnetoelectric coefficient (α) of poled 34PTDy10 as a function of frequency.

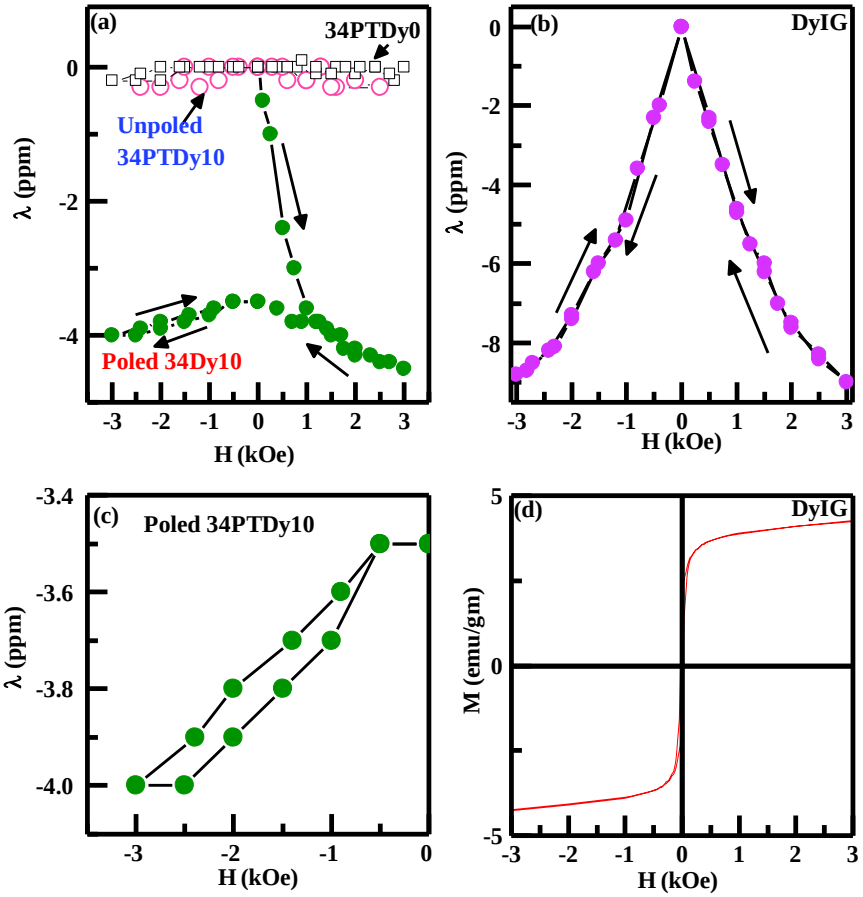

FIG. 4. (a) Room temperature magnetostriction of 34PTDy10 in poled (green solid circles) and unpoled (pink open circles) condition. The magnetostriction of 34PT sample is represented by open black squares. (b) Magnetostriction of DyIG at room temperature. (c) Expanded region of magnetostriction of 34PTDy10. (d) M-H loop for DyIG at room temperature.